Nuclear Instruments and Methods in Physics Research B 111 (1996) 195-208

ELSEVIER

NIM B
Beam Interactions
with Materials & Atoms

A hybrid multiple-scattering theory for electron-transport Monte Carlo calculations

Alex F. Bielajew *

Institute for National Measurement Standards, National Research Council of Canada, Ottawa, K1A 0R6 Canada

Received 14 September 1995; revised form received 27 October 1995

Abstract

This paper describes a new elastic multiple-scattering theory and its incorporation into the EGS4 Monte Carlo code. The important features of the new theory are: 1) the angular distributions are stable physically and numerically from the no-scattering small electron pathlength limit to the multiple scattering regime where electron pathlengths can be thousands of mean-free-paths long, 2) in the small-pathlength limit, the angular distributions may be made to conform to an arbitrary cross section. The object of this paper is to describe the implementation and show results that demonstrate its stability by comparing with distributions generated from a single elastic-scattering model and by showing convergence of backscatter calculations.

1. Introduction

Certain classes of condensed-history Monte Carlo electron transport calculations require that the electron angular distributions arising as a result of cumulative elastic Coulomb scattering be stable over a large range of pathlengths. This stability means that the electron path-length may be divided up into an arbitrary number of substeps with the resulting angular distribution independent of how the substeps were generated. One important example of an application requiring this stability is the calculation of thick-walled ion chamber response [1–8]. Artefacts associated with step-size stability in ion chamber calculations have led to much discussion [9–14].

A systematic attempt to heal the instability problem was made by Bielajew and Rogers [15,16] in the development of PRESTA (the Parameter Reduced Electron-Step Transport Algorithm). However, that work was influenced by the small step-size constraint of the Molière multiple elastic-scattering theory [17,18] which causes errors of the order of 6–7% for step-sizes 20 mean-free-paths in length [19,20] and gets progressively worse for smaller step-sizes. The Molière theory breaks down mathematically for step-sizes less than about 5 mean-free-paths where the angular distributions become negative. Below about 3 mean-free-paths the Molière distributions cannot be defined owing to divergence of one of the Molière parameters. Ionisation chamber cavities are of the order of a few mean-free-paths for the typical electron that crosses it. Thus, it is not surprising that the calculation of ionisation chamber response is not completely resolved given the current physics' modeling of the PRESTA algorithm [21–23,8].

The artefacts in ionisation chamber response have been related to an inadequate response in backscatter from the downstream wall of the chamber [22,23]. As well, other shortcomings in the PRESTA algorithm not directly related to the angular distributions [24,25,8] have been discussed. To some extent these defects are related to longitudinal and lateral displacements, and other details of how the scattering algorithms are invoked play a role in the stability of ionisation chamber calculations. However, these are beyond the scope of this report and will be addressed in other publications. Before these other problems are addressed, the lower step-size constraint of the multiple-scattering theory must be removed and the algorithms included in a Monte Carlo code. This is the aim of this report — to introduce a new multiple-scattering theory and to demonstrate its performance in a Monte Carlo code. This new multiple-scattering theory is based upon a recently developed small-angle theory [20] but allows the angular distributions in the small-pathlength limit to conform to an arbitrary elastic scattering cross section. As accurate ionisation-chamber response requires the accurate modeling of backscatter, the new theory is tested by comparing with single elastic-scattering calculations.

* Tel. +1 613 993 2197, fax +1 613 952 9865, e-mail alex@irs.phy.nrc.ca.

SSDI 0168-583X(95)01337-7

2. Formulation of the new theory

In a previous paper [20] a new small-angle multiple-scattering distribution was introduced. It has the form:

$$f(\Theta,\lambda)\Theta\,\mathrm{d}\Theta = \mathrm{e}^{-\lambda}\delta(\Theta)\,\mathrm{d}\Theta + (1-\mathrm{e}^{-\lambda})\,q^{(1)}(u,\lambda,\omega)\,\mathrm{d}u, \tag{1}$$

where $f(\Theta,\lambda)$ is the distribution of scattering angles Θ as a function of the pathlength λ measured in units of mean-free-path, $\delta(\Theta)$ is the Dirac delta function, $q^{(1)}(u,\lambda,\omega)$ is the distribution that describes the conditional probability that at least one scattering has occurred and it is a function of a transformed angle variable $u = 1 - \chi_\alpha^2\omega^2/(\Theta^2+\chi_\alpha^2\omega^2)$, the pathlength λ, a "spreading" parameter ω that is chosen to make $q^{(1)}(u,\lambda,\omega)$ as flat as possible, and χ_α which is the screening angle (itself a function of the electron energy and the atomic number of the target). Using the small-angle form of the screened Rutherford cross section, $\sigma(\Theta) \propto (\Theta^2+\chi_\alpha^2)^{-2}$, $q^{(1)}(u,\lambda,\omega)$ has been determined numerically within the "exact" small-angle multiple scattering formalism of Bothe [26] and Wentzel [27] (the small-angle counterpart to the "exact" any-angle formalism of Goudsmit and Saunderson [28,29]) over the range $0 \le \lambda \le 3050.53$.

The hybrid multiple-scattering theory given in this paper is an extension of the theory described above and can apply over the same range of pathlengths. The motivation for developing the present approach was that in the previous treatment backscatter results would not converge those of the any-angle form of the screened Rutherford elastic cross section because the best that could be accomplished by the use of Eq. (1) was the small-angle form of the cross section. The development described below eliminates this shortcoming.

The starting point is the Goudsmit–Saunderson formalism [28,29]):

$$f(\Theta,\lambda)\sin\Theta\,\mathrm{d}\Theta = \mathrm{e}^{-\lambda}\sum_{l=0}^{\infty}(l+\tfrac{1}{2})\mathrm{e}^{\lambda g_l}P_l(\cos\Theta)\sin\Theta\,\mathrm{d}\Theta, \tag{2}$$

where $P_l(\cos\Theta)$ is the Legendre polynomial of order l. The distance λ measured in mean-free-path's is related to the cross section $\sigma(\Theta)$ by:

$$\lambda = \frac{2\pi N_A t}{A}\int_0^{\pi}\mathrm{d}\Theta\,\sin\Theta\sigma(\Theta), \tag{3}$$

where N_A is Avogadro's number, A is the atomic weight, t is the pathlength given in g/cm^2, and $\sigma(\Theta)$ is arbitrary at this stage. The g_l factors are defined by:

$$g_l = \int_0^{\pi}\mathrm{d}\Theta\,\sin\Theta\tilde{\sigma}(\Theta)P_l(\cos\Theta), \tag{4}$$

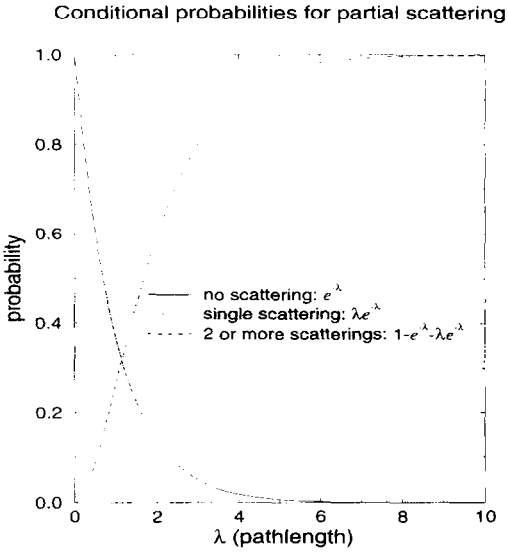

Fig. 1. Probabilities for no scattering, single scattering and two or more scatterings as made explicit by Eq. (6).

and the normalised cross section $\tilde{\sigma}(\Theta)$ by:

$$\tilde{\sigma}(\Theta) = \sigma(\Theta)\Big/\int_0^{\pi}\mathrm{d}\Theta\,\sin\Theta\sigma(\Theta). \tag{5}$$

If one makes an expansion within the summand of Eq. (2) adding and subtracting terms to keep the expression exact, one can write:

$$f(\Theta,\lambda) = \mathrm{e}^{-\lambda}\delta(1-\cos\Theta) + \lambda\mathrm{e}^{-\lambda}\tilde{\sigma}(\Theta) + (1-\mathrm{e}^{-\lambda}-\lambda\mathrm{e}^{-\lambda}) \times\sum_{l=0}^{\infty}(l+\tfrac{1}{2})P_l(\cos\Theta)\frac{\mathrm{e}^{\lambda g_l}-1-\lambda g_l}{\mathrm{e}^{\lambda}-1-\lambda}. \tag{6}$$

The first term (proportional to $\mathrm{e}^{-\lambda}$) represents the conditional probability that no scattering has occurred. The second term (proportional to $\lambda\mathrm{e}^{-\lambda}$) represents the conditional probability that only one scattering has occurred. The third term (proportional to $1-\mathrm{e}^{-\lambda}-\lambda\mathrm{e}^{-\lambda}$) represents the conditional probability that only two or more scatterings have occurred. The relative contributions of these three terms is shown in Fig. 1. Eq. (6) is an exact rewrite of Eq. (2). The only difference is that the no-scattering and first-scattering terms are made explicit. Apart from notation, this is the same expression given by Berger and Wang [30] who proposed this form as a way of making the Goudsmit–Saunderson series converge more rapidly for large l, a well-known difficulty that must be handled delicately [31].

The explicit extraction of the single-scattering term suggests the adjective "hybrid" since in the regime of small pathlengths the multiple-scattering distribution is dominated explicitly by the single-scattering distribution. This may be exploited by geometry-adaptive electron-transport algorithms

such as PRESTA [15,16] or Seltzer's TLC (Transverse and Longitudinal Correction) [32] to effect the crossing of material (or scoring) boundaries. As a boundary is approached the condensed-history algorithm "evaporates" into a single-scattering algorithm. The combination of single-scattering and multiple-scattering algorithms into a single formalism is therefore a hybrid method that can exploit both the computational efficiency of multiple-scattering theories with the accuracy of a single-scattering approach.

The extraction procedure may be extended further, developing terms of the form $\lambda^n e^{-\lambda} f^{(n)}(\Theta)/n!$ where $f^{(n)}(\Theta)$ is the conditional probability that exactly n scatterings has occurred.[1] We have seen from general considerations that $f^{(0)}(\Theta) = \delta(1-\cos\Theta)$ and $f^{(1)}(\Theta) = \tilde{\sigma}(\Theta)$ where $\tilde{\sigma}(\Theta)$ is completely arbitrary. Eq. (6) is preferable because numerical calculations of $f^{(n)}(\Theta)$ would have to be performed for each value of n for $n \geq 2$. The order of difficulty of these numerical calculations would be about the same as the numerical calculation of two-or-more term of Eq. (6) and additional calculation and complexity would be introduced to the Monte Carlo transport algorithm. Eq. (6) is the simplest form that yields the exact form of the single-scattering cross section in the small pathlength limit whereas Eq. (2) can only yield the small-angle form of the cross section.

The multiple-scattering distribution described by Eq. (6) is to be adapted to the EGS4 Monte Carlo code [33,34] and thus certain approximations are made. The normalised cross section $\tilde{\sigma}(\Theta)$ is associated with the screened Rutherford cross section that is proportional to $(1-\cos\Theta+\chi_\alpha^2/2)^{-2}$ and given by:

$$\tilde{\sigma}(\Theta) = \frac{2\chi_\alpha^2(1+\chi_\alpha^2/4)}{(2-2\cos\Theta+\chi_\alpha^2)^2}. \tag{7}$$

The screening angle χ_α is associated with Molière's screening angle [17]. This is given in Berger and Wang's notation [30] as:

$$\chi_\alpha^2 = \frac{6.8\times10^{-5}Z^{2/3}}{\tau(\tau+2)}(1.13+3.76\alpha^2), \tag{8}$$

where Z is the atomic number, τ is the electron's kinetic energy in units of its rest mass energy and $\alpha = Z/137\beta$, where β is the electron's speed as a fraction of the speed of light. EGS4 makes the further assumption that $\beta = 1$ in its form of the screening angle. Although it would be easy to relax this latter assumption in EGS4 at the loss of some computational efficiency, it would seem premature without further study. Seltzer [31] has recommended that the $1/\beta^2$ implied in Eq. (8) be replaced by $\sqrt{\tau/(\tau+1)}/\beta^2$, an elegant empirical correction factor that makes the screened Rutherford cross section conform much more closely to the more accurate Mott cross section [35,36] that contains spin and relativistic effects. At low energies, this implies that the $1/\beta^2$ should be replaced by $\frac{1}{2}\beta$, a much weaker dependence. Nonetheless, the approximation made to the screening angle by EGS4 is under question and ought to be revised after further investigation.

The final approximation is to evaluate the two-or-more scattering term of Eq. (6) in the small-angle approximation. Thus,

$$\begin{aligned} f^{(2+)}(\Theta,\lambda) &= \sum_{l=0}^{\infty}(l+\tfrac{1}{2})P_l(\cos\Theta)\frac{e^{\lambda g_l}-1-\lambda g_l}{e^\lambda-1-\lambda} \\ &\approx \sqrt{\frac{\Theta}{\sin\Theta}}\int_0^\infty d\nu\,\nu J_0(\nu\Theta)\frac{e^{\lambda g(\nu)}-1-\lambda g(\nu)}{e^\lambda-1-\lambda}, \end{aligned} \tag{9}$$

where J_0 is the zeroth-order Bessel function of the first kind and

$$g(\nu) = \chi_\alpha\nu K_1(\chi_\alpha\nu), \tag{10}$$

where K_1 is the first-order modified Bessel function of the second kind.

There are several steps and approximations that have been used to obtain Eqs. (9) and (10). Both Bethe [37] and Winterbon [38] have discussed some of these approximations and have provided further corrections. The first is the conversion of the summation to an integral using the Euler summation formula [39]. The first-order approximation $\sum_{l=0}^{\infty}F(l+\frac{1}{2}) \approx \int_0^\infty d\nu\,F(\nu)$ was employed. The Legendre function $P_l(\cos\Theta)$ was approximated by $P_l(\cos\Theta) \approx \sqrt{\Theta/\sin\Theta}J_0[(l+\frac{1}{2})\Theta]$. The small-angle conversion of the factor in the exponential may be derived in several ways. The simplest method [20] is to use the small-angle form for the normalised cross section $\tilde{\sigma}(\Theta) \approx 2\chi_\alpha^2/(\Theta^2+\chi_\alpha^2)^2$ normalised such that $\int_0^\infty\tilde{\sigma}(\Theta) = 1$, and substituting $\sin\Theta P_l(\cos\Theta) \approx \Theta J_0[(l+\frac{1}{2})\Theta]$ in Eq. (4). Alternatively, with the use of the general from of the screened Rutherford cross section, the integral in Eq. (4) may be done yielding:

$$g_l = -\chi_\alpha\sqrt{1+\chi_\alpha^2/4}\,Q_l^1(1+\chi_\alpha^2/2), \tag{11}$$

where Q_l^1 is the first-order associated Legendre function of the second kind chosen so that the branch cut lies between 1 and $-\infty$. It is then possible to relate these functions with the K_1 function [40] in the same way the P_l's and the J_0's are related. This leads to a consistent manner of improving upon the simple approximation but is not pursued further herein.

The small-angle form of the multiple scattering distribution,

$$f_{SA}^{(2+)}(\Theta,\lambda)\Theta\,d\Theta = d\Theta\,\Theta\int_0^\infty d\nu\,\nu J_0(\nu\Theta)\frac{e^{\lambda g(\nu)}-1-\lambda g(\nu)}{e^\lambda-1-\lambda}, \tag{12}$$

[1] This is known from elementary probability theory. However, a new derivation of the Goudsmit–Saunderson series starting from a summation of conditional probabilities is given in the Appendix.

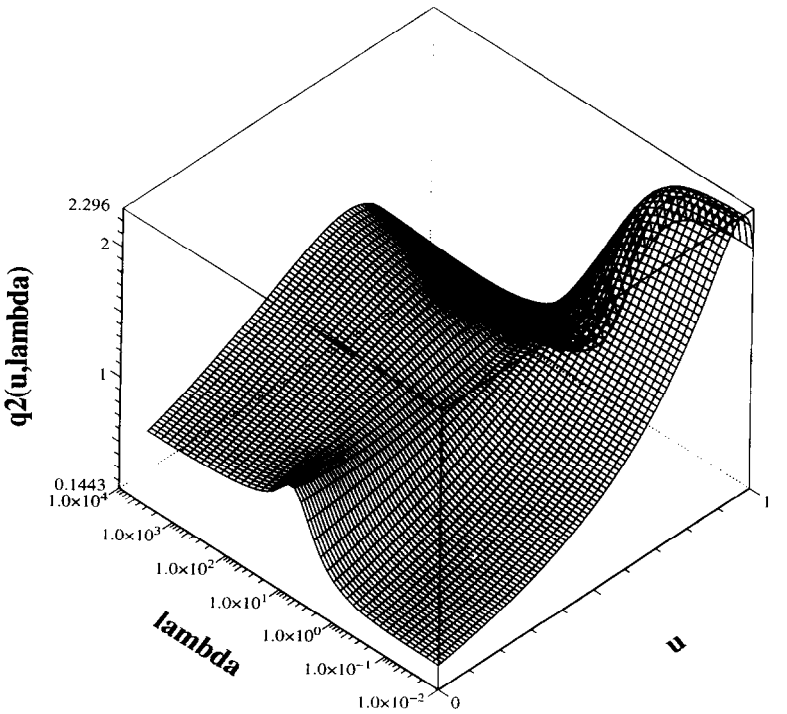

Fig. 2. The $q^{(2)}(u, \lambda, \omega)$ function vs. λ and u.

has the normalisation property,

$$\int_0^\infty \mathrm{d}\Theta\, \Theta f_{\mathrm{SA}}^{(2+)}(\Theta, \lambda) = 1, \tag{13}$$

and in the limit of small λ attains the small-angle two-scattering limit [20]:

$$\lim_{\lambda \to 0} f_{\mathrm{SA}}^{(2+)}(\Theta, \lambda)\Theta \mathrm{d}\Theta = \left(\frac{2\xi \mathrm{d}\xi}{3}\right) {}_2F_1\left(2, 3; \frac{5}{2}; \frac{-\xi^2}{4}\right), \tag{14}$$

where $\xi = \Theta/\chi_a$, and ${}_2F_1(\,)$ is the hypergeometric function. [2]

Following the procedure developed previously [20], a transformation of variables $u = 1 - \omega^2/(\xi^2 + \omega^2)$ is adopted, where for the moment ω is arbitrary. Thus,

$$f_{\mathrm{SA}}^{(2+)}(\Theta, \lambda)\Theta \mathrm{d}\Theta = q^{(2)}(u, \lambda, \omega)\, \mathrm{d}u, \tag{15}$$

in analogy with the $q^{(1)}(u, \lambda, \omega)$ function of the previous paper that contained the single-scattering distribution as well, but in small angle form. The ω of the previous paper was chosen to make $q^{(1)}(u, \lambda, \omega)$ as flat as possible. Rather than re-calculate ω with a similar procedure, the ω of the previous paper is adopted. This makes the $q^{(2)}(u, \lambda, \omega)$ surface not optimally flat for small λ but it allows one to relate $q^{(1)}(u, \lambda, \omega)$ and $q^{(2)}(u, \lambda, \omega)$ quite easily. One can easily construct $q^{(1)}(u, \lambda, \omega)$ from $q^{(2)}(u, \lambda, \omega)$ by adding the small-angle form of the cross section transformed into the u variable. This was done to check the numerical procedure involved in the calculation of $q^{(2)}(u, \lambda, \omega)$ while $q^{(1)}(u, \lambda, \omega)$ has been verified independently using a Monte Carlo calculation formulated in a small-angle transport formalism [20].

The $q^{(2)}(u, \lambda, \omega(\lambda))$ (u, λ)-surface was computed over the range $0.01 \leq \lambda \leq 3050.53$ with a mesh-density of 64 logarithmically-spaced points per decade in λ and 101 uniformly-spaced points spanning u. The results are plotted in Fig. 2. For each λ, cubic-spline coefficients were computed [42] and these were used to form the cumulative probability distribution:

$$c(u, \lambda) = \int_0^u q^{(2)}(u, \lambda, \omega(\lambda))\, \mathrm{d}u', \tag{16}$$

and fit with cubic splines. Finally, with the intent of rapid sampling within the Monte Carlo code, the inverse cumulative probability distribution was formed, allowing the determination of u knowing c and λ. A table with the same mesh density in c and $\log(\lambda)$ was constructed for linear in-

[2] The mathematical notation used in this report follow those of Wolfram [41] and the Mathematica code system was employed for most of the numerical computations reported herein.

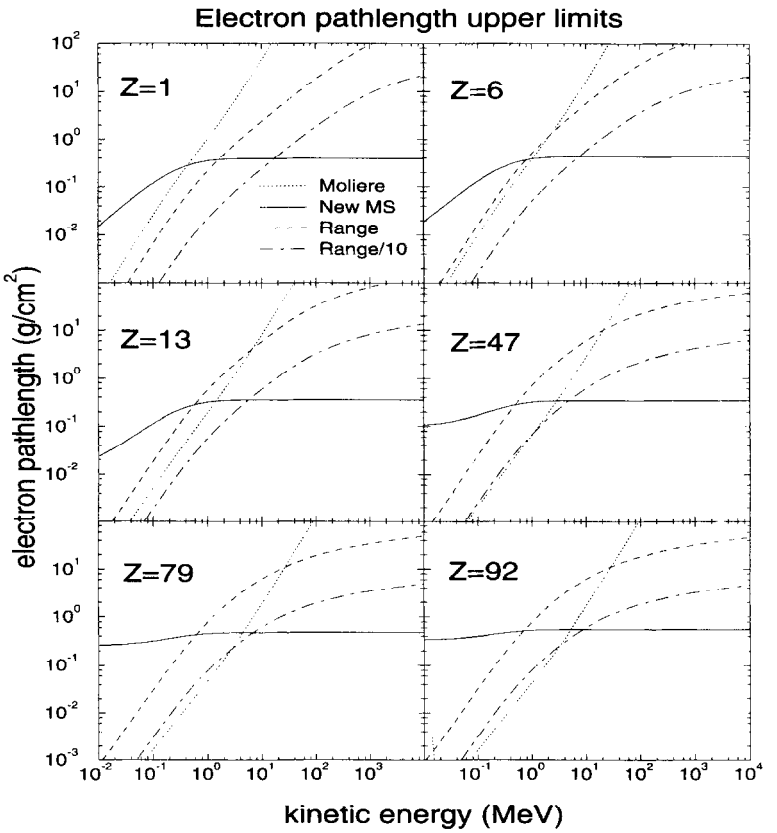

Fig. 3. Comparison of the upper limits provided by the Molière theory (dotted line), the new theory (solid line) the CSDA range (dashed line) and one tenth the CSDA range.

terpolation in the determination of u. For $\lambda < 0.01$, linear interpolation was used between the known $\lambda = 0$ limit expressed by Eq. (14) and $q^{(2)}(u, 0.01, \omega(0.01))$. A cubic-spline interpolation scheme was employed for determining ω as a function of λ.

Gathering the results at this point, the multiple-scattering distribution employed is:

$$f(\Theta,\lambda)\sin\Theta\,d\Theta = e^{-\lambda}\delta(1-\cos\Theta)\sin\Theta\,d\Theta + \lambda e^{-\lambda}\tilde{\sigma}(\Theta)\sin\Theta\,d\Theta + (1-e^{-\lambda}-\lambda e^{-\lambda})\sqrt{\frac{\sin\Theta}{\Theta}}q^{(2)}(u,\lambda,\omega(\lambda))\,du. \quad (17)$$

The sampling procedure employed the following prescription:

(i) λ is given as the pathlength to be transported.
(ii) Choose a random number ξ_1 such that $0 \le \xi_1 \le 1$.
(iii) If $\xi_1 \le e^{-\lambda}$, a no-scattering event has occurred. Without deflection, transport the electron a distance λ.
(iv) Else, if $\xi_1 \le (1+\lambda)e^{-\lambda}$, a single-scattering event has occurred. Transport the electron a distance λ and deflect the particle according to the normalised single-scattering cross section given in Eq. (7). (It is possible to do this directly by forming the cumulative probability distribution and inverting.)
(v) Else, a multiple-scattering event has occurred. Choose a second random number ξ_2 such that $0 \le \xi_2 \le 1$ and use it to extract a value of u from the inverse cumulative distribution table described above. Calculate $\omega(\lambda)$ using the cubic-spline interpolation constants and use this as well as χ_α to determine Θ. If $\Theta > \pi$, repeat step 5. Account for the $\sqrt{\sin\Theta/\Theta}$ factor using a rejection technique. That is, choose a third random number ξ_3 such that $0 \le \xi_3 \le 1$. If $\Theta\xi_3^2 > \sin\Theta$, repeat step 5. Transport the electron a distance λ and deflect it using the selected angle Θ.

It should be emphasized that although the Molière screening angle and the screened Rutherford elastic cross section were employed for this work, the theory is more general. Indeed, any cross section may be employed for the single-scattering part, that proportional to $\lambda e^{-\lambda}$ in Eq. (6). For example, partial-wave single-scattering cross sections have been employed in the EGS4 code [43]. The multiple scattering part is still couched in the small-angle formalism but, as discussed previously [20], the screening angle and total cross

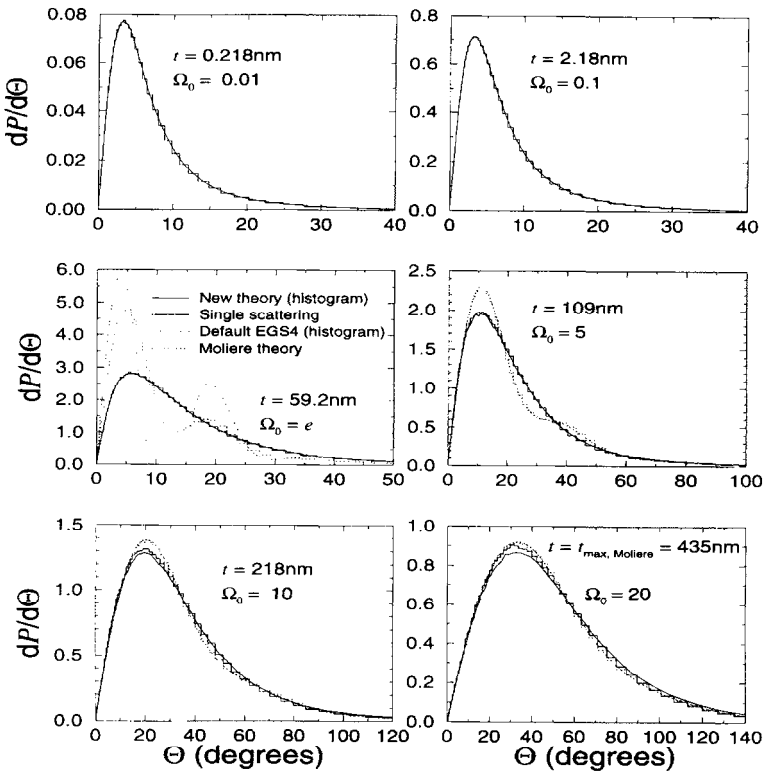

Fig. 4. Multiple scattering angular distributions, $dP/d\Theta$, for 6.8 keV electrons in graphite vs. Θ for total distances ranging from $t = 0.218$ nm to $t = 435$ nm ($\Omega_0 = 20$, the lower physical bound for Molière theory and also the maximum step-size for this energy). Also shown is the distance $t = 59.2$ nm corresponding to $\Omega_0 = e$, the minimum electron step-size allowed by Molière theory. The solid histogram is the new multiple-scattering theory, the solid line is the single-scattering simulation using a screened Rutherford cross section. The dotted histogram is the default EGS4 sampling of the Molière multiple-scattering theory. The dotted line is the prediction of Molière theory. All multiple-scattering distributions have been corrected by the large-angle $\sqrt{(\Theta/\sin\Theta)}$ correction.

sections in this part of the distribution may be considered arbitrary and fit to the first and second transport cross sections of more accurate single-scattering theories.

In Fig. 3 the upper pathlength limit of the aforementioned new theory is compared with that of Molière theory.[3] The Molière upper limit was proposed by Bethe [37] to keep the average angle below one radian. The upper limit of the exact theory is determined by the upper limit that could be computed numerically[4] corresponding to $\lambda = 3050.53$. Fig. 3 shows that the conclusions are quite similar for all target materials from hydrogen to uranium. The limit of the new theory is about 0.4 g/cm^2 at relativistic energies and somewhat smaller for non-relativistic energies. In realistic applications energy-loss considerations are the determining factor for setting pathlengths to be used. Therefore, pathlengths corresponding to the full range as calculated in the continuous slowing down approximation (CSDA) [44–46] as well as one-tenth of this range are also shown in the figure. One can conclude that the smaller upper pathlength limit of the new theory is not an actual limitation below about 10 MeV.

3. Results

3.1. Angular distributions

Multiple and single-scattering angular distributions $dP/d\Theta$ are depicted in Figs. 4–12 for three materials, C, Al and Au, for three different energies for pathlengths measured in terms of Ω_0 of Molière theory. ($\Omega_0 = 0.857\lambda$.) The uppermost energy in each case is 1 MeV while the lowest energy corresponds to the case $\Omega_0 = 20 = \Omega_{max}$, where Ω_{max} is the maximum pathlength for which Bethe [37] considered the Molière theory to be valid. Molière considered his theory valid for $\Omega_0 > 20$ [18]. In each case angular distributions for $\Omega_0 = 20$ and $\Omega_0 = \Omega_{max}$ are shown as well as those for $\Omega_0 = e$ where Molière theory reaches a mathematical lower bound. The distributions at an intermediate value of $\Omega_0 = 5$ and two values below the $\Omega_0 = e$ barrier

[3] This discussion also applies to the small-angle formalism described in the previous paper [20].

[4] While it may be possible to recast the equations into a form that would be stable numerically for larger pathlengths, there is little motivation to do this either from the standpoint of accuracy or computational efficiency. The Molière theory yields distributions that are less than 1% inaccurate for $\lambda > 3000$ and sampling from either distribution can be accomplished with equal computational speed.

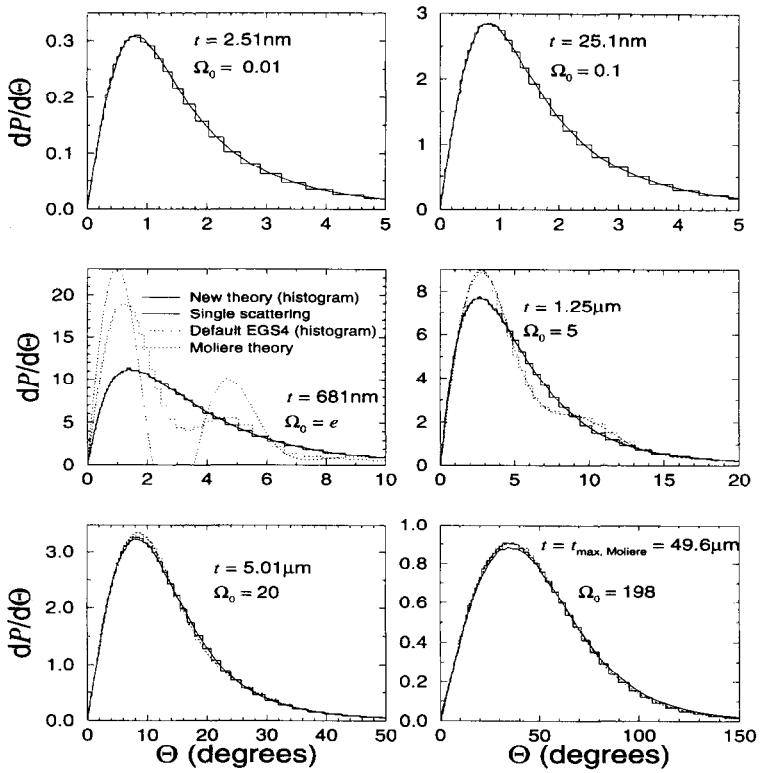

Fig. 5. Multiple scattering angular distributions for 100 keV electrons in graphite.

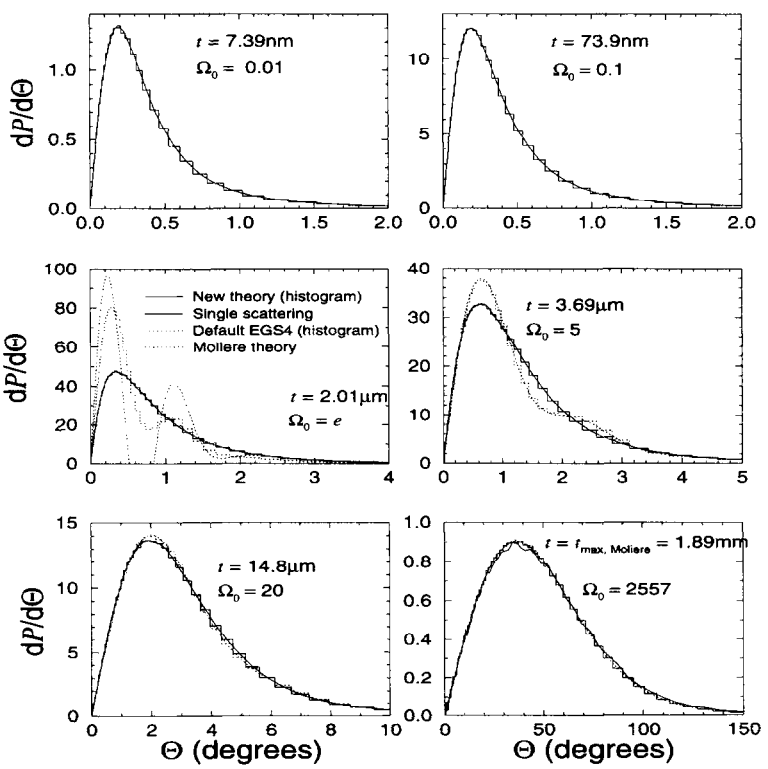

Fig. 6. Multiple scattering angular distributions for 1.0 MeV electrons in graphite.

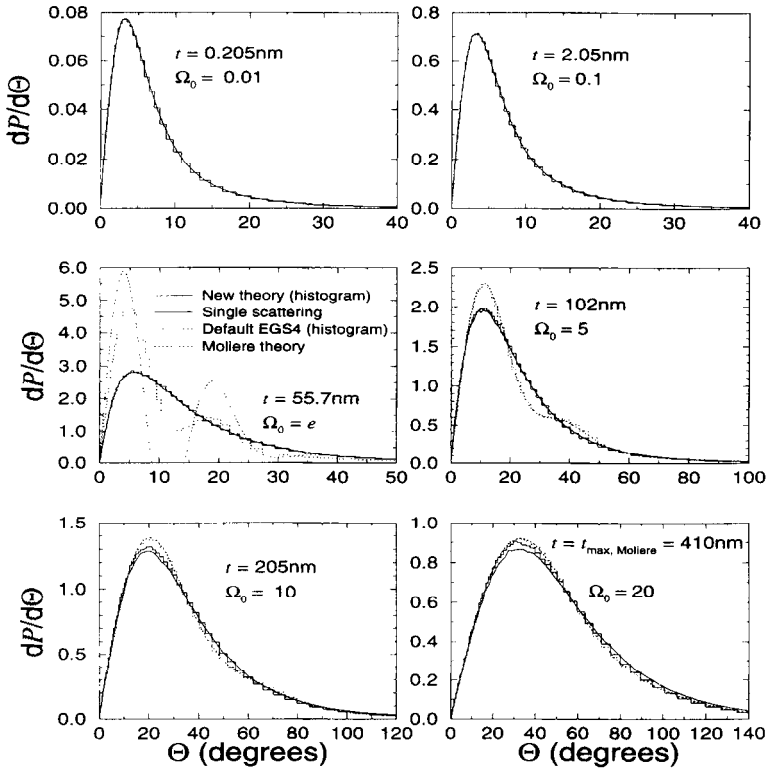

Fig. 7. Multiple scattering angular distributions for 11.60 keV electrons in aluminum.

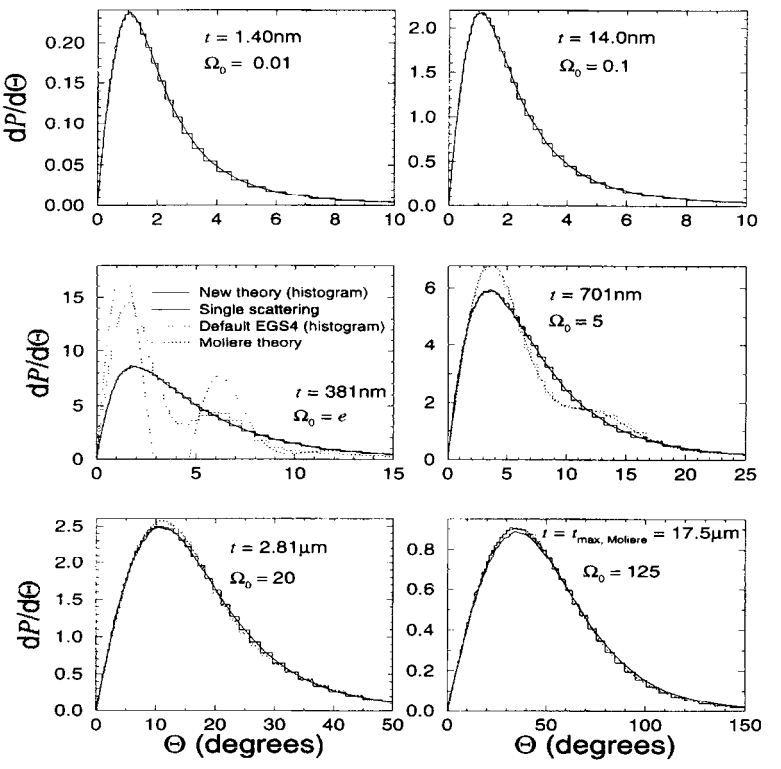

Fig. 8. Multiple scattering angular distributions for 100 keV electrons in aluminum.

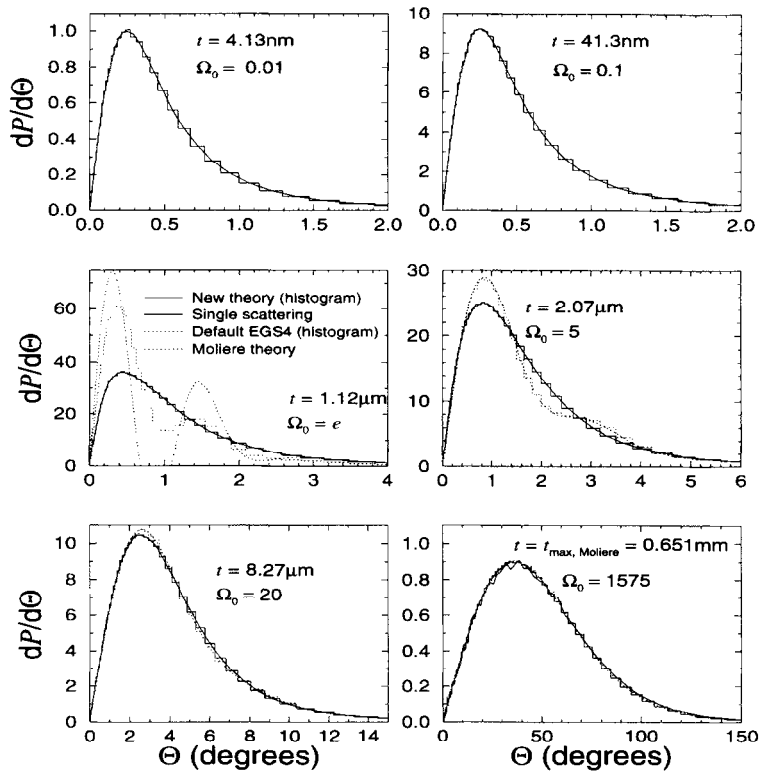

Fig. 9. Multiple scattering angular distributions for 1.0 MeV electrons in aluminum.

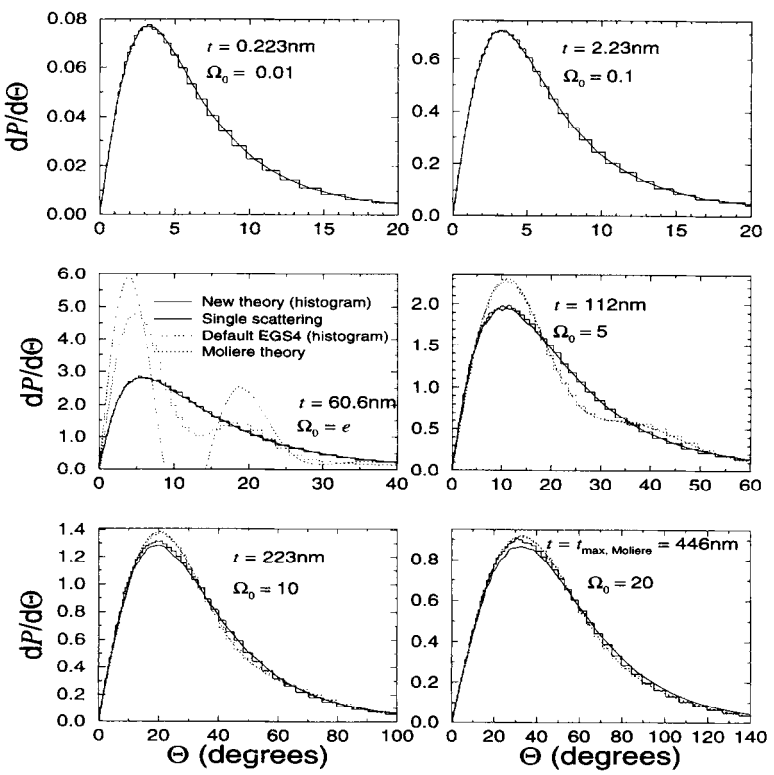

Fig. 10. Multiple scattering angular distributions for 74.6 keV electrons in gold.

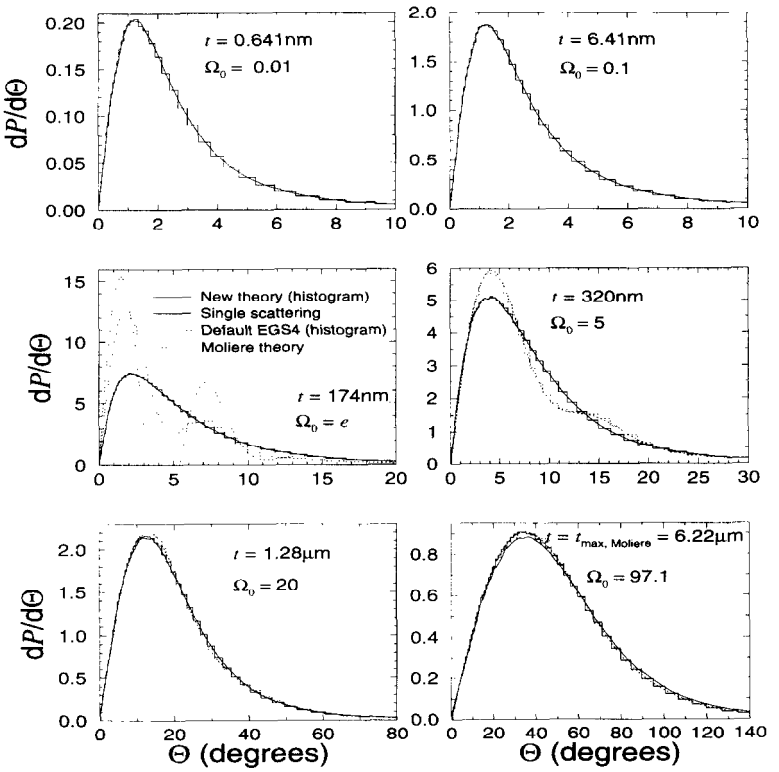

Fig. 11. Multiple scattering angular distributions for 400 keV electrons in gold.

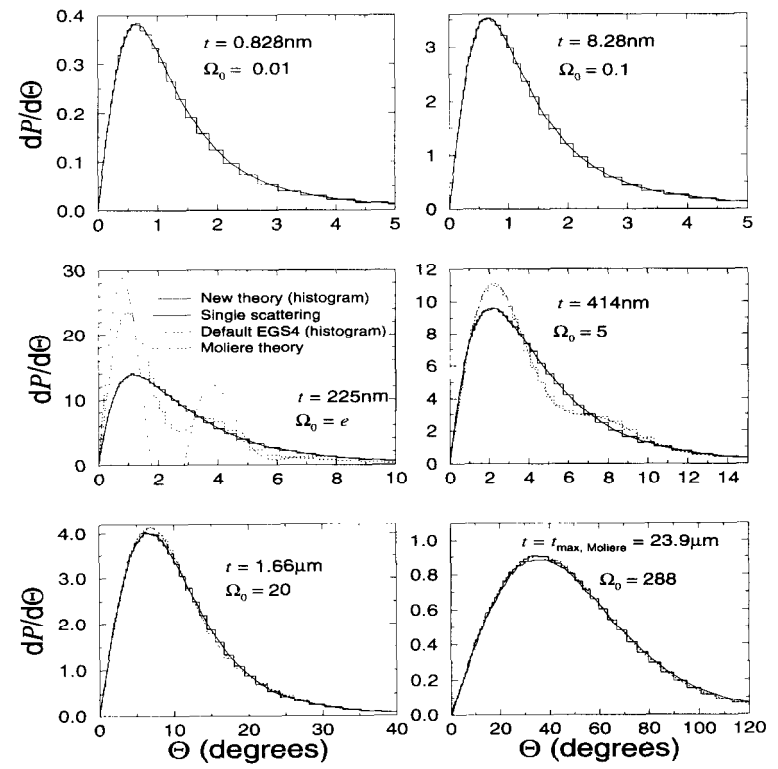

Fig. 12. Multiple scattering angular distributions for 1.0 MeV electrons in gold.

are depicted as well.

The predictions of the new multiple-scattering theory described in this work are depicted by the solid-line histograms. The results of the any-angle screened Rutherford cross section are shown by the solid lines. The results of the EGS4 Monte Carlo calculations are shown by the dashed-line histograms and the results of the Molière theory by the dashed lines. The three multiple-scattering histograms or curves are corrected by the $\sqrt{\Theta/\sin\Theta}$ correction factor. There was no energy loss in these simulations and the screening angle employed was that used by EGS as described below Eq. (8). Each curve represents one million particle histories that have scattered at least once. The no-scattering results are not shown.

The following features may be noted. For pathlengths $\Omega_0 = 5$ and below, the new multiple-scattering theory and single-scattering results are in excellent agreement. For larger pathlengths and lower energies, a slight difference appears between the new theory and the single scattering results. The single-scattering distributions are somewhat wider. This suggests that either the large-angle $\sqrt{\Theta/\sin\Theta}$ correction is inadequate to the task or that the difference arises from the approximation introduced in the exponent in Eq. (9). The apparent χ_α-dependence of this difference supports this argument. One may derive Molière theory from an expansion in χ_α of Eq. (11) and there would be extra terms of higher order in χ_α that may contribute to a further correction. Another approach would be to use the relation between the modified Bessel functions and the associated Legendre functions [40] that connects Eqs. (10) and (11) with higher-order terms in χ_α. For this work, the newer corrections are not developed but reserved for possible future work. The new multiple-scattering theory in its present form provides the promise of attaining accurate results in the limit of small pathlength and provides a significant improvement over Molière theory at small pathlength.

The agreement between the new theory and the single-scattering results is better for all pathlengths shown except for pathlengths such that $\Omega_0 \gg 20$ where the new theory and Molière's theory converge to the same answer. This is to be expected as the differences between the new theory and Molière's theory become smaller with increasing pathlength [20]. One can also note the agreement between the distributions produced by standard EGS and the Molière distribution. Even the onset of spurious wiggles at $\Omega_0 = 5$ is matched by the Monte Carlo sampling routines. However, at $\Omega_0 = e$ the Monte Carlo sampling routines "smooth over" the large amplitude oscillations produced by Molière's theory in an inappropriate mathematical regime.

3.2. Transmission calculations

The pathlength stability of transmission was studied for electrons with energies between 10 keV and 10 MeV incident normally on a semi-infinite "slab" of water. The energy-loss model employed was the "continuous slowing down approximation" (CSDA). No secondary particles were created and particles lost energy via total collision and radiative stopping powers until the electrons traveled a total distance equal to the CSDA range r_0. The fractional energy deposited beyond $r_0/2$ is shown in Fig. 13 as a function of the electron step-size calculated in terms of the fractional energy lost per step (ESTEPE) [47]. This is the same calculation done in demonstration of PRESTA's step-size stability [15,16] except that modern computers have permitted the accumulation of better statistics and the examination of very small pathlengths.

The calculations employed the latest version of the PRESTA algorithm with its intrinsic Molière modeling of the deflection angles, mid-point energy averaging, lateral sub-step deflection and accurate pathlength (detour) corrections. These results are represented by circles. The filled circle is the default PRESTA result without ESTEPE control while the open circles apply the additional ESTEPE restriction. Once the step-size is so small that the Molière distributions become overly forward directed, the energy deposition in the downstream slab becomes artificially high. At 10 MeV, however, the PRESTA algorithm does not show the anomaly even at the smallest pathlength shown of about 4 mean free paths.[5] With the incorporation of the new multiple-scattering theory (shown by the diamond symbols), the results converged to the single-scattering result which used the any-angle screened Rutherford cross section (depicted by the square symbol). The exception is the 10 MeV case which had not yet converged.

The source of the remaining step-size dependence, amounting to a few percent, is not yet known. It is unlikely that it is due to the remaining differences between the single-scattering and the new multiple-scattering distributions since the step-size dependence occurs for all energies and has a similar shape. A re-examination of the longitudinal and lateral sub-step distributions is called for and is left for future work.

3.3. Backscatter calculations

A similar calculation was done as in the previous section except that the fractional energy backscattered from the semi-infinite water slab was accumulated. The results are shown in Fig. 14. Without ESTEPE control both the PRESTA algorithm and the new multiple scattering theory underpredict backscatter. As the step-size is made smaller the PRESTA results never converge to the single-scattering result because of the small step-size inadequacy of the Molière theory. In contrast, the new theory converges to the single-scattering result.

[5] The ESTEPE = 1×10^{-4} cases took longer than one CPU-day to compute on a modern desktop workstation, dampening the motivation to demonstrate the artefact.

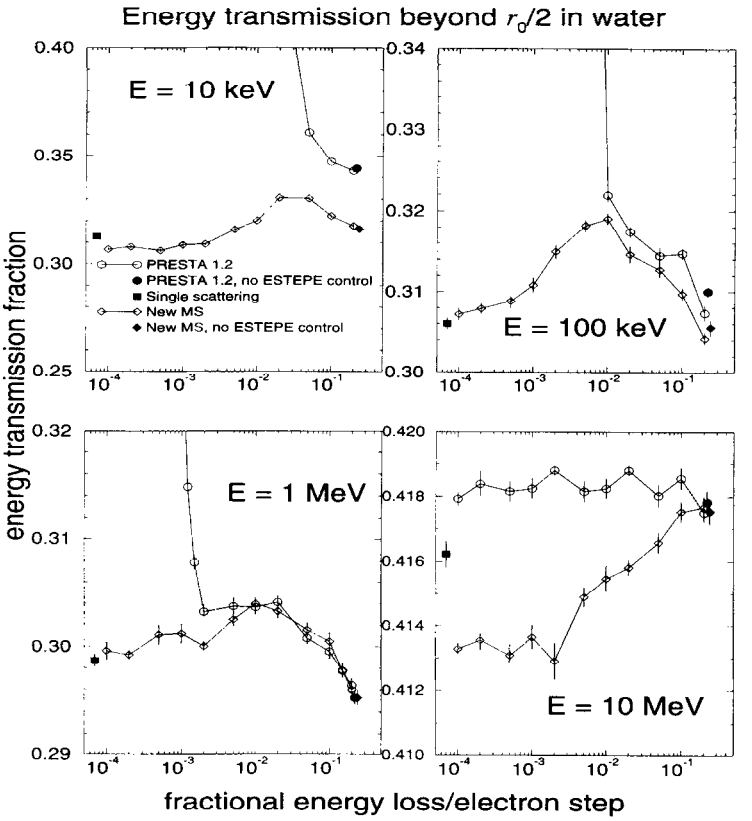

Fig. 13. Energy deposition beyond the $r_0/2$ point in water.

4. Conclusions

A new multiple-scattering theory has been developed that provides angular distributions that are consistent in the sense that the electron pathlengths may be divided up in an arbitrary manner and the resulting distributions are the same.

It should be remarked at this point while the results converge to the single-scattering results, the answer may not be correct! This is so because an approximate form of the elastic cross section was employed. Transmission and backscatter results may depend to some extent on the details of a more accurate cross section. Moreover, at very low energies the CSDA approximation is invalid [30]. This is because at very low energies the energy-loss mechanisms are catastrophic — few events with large fractional changes in energy. It has been shown that to model backscattering accurately at low energy one must model energy-loss discretely with a single inelastic scattering model [48]. However, the purpose of the present work has been to find an approach to get *consistency* over a wide range of electron pathlengths. A lack of consistency is the major reason why ion chamber calculations can fail as the electrons within an ion chamber are in a state of quasi-equilibrium [49] and large changes in density from the chamber walls to the cavity gas cause almost no perturbation [50]. An inconsistent multiple-scattering theory *manufactures* disequilibrium. The newer consistent theory provides a tool for doing accurate simulations of ion chambers.

As remarked previously, one may use an arbitrary cross section and be guaranteed that in the limit of small step-size, calculated results will converge to single-scattering results. Yet, even with the use of an approximate cross section the remaining step-size dependencies of backscatter calculations motivates the search for the cause. If the goal of algorithm design is to minimise the dependence on step-size, it is clear that there is much work to be done. The areas left to be investigated are: 1) remaining differences between the multiple and single scattering distributions, 2) accurate lateral correlation and straggling algorithms, and 3) accurate longitudinal correlation and straggling algorithms. Only after these problems are surmounted can we consider moving on to the problem of using more sophisticated elastic cross sections.

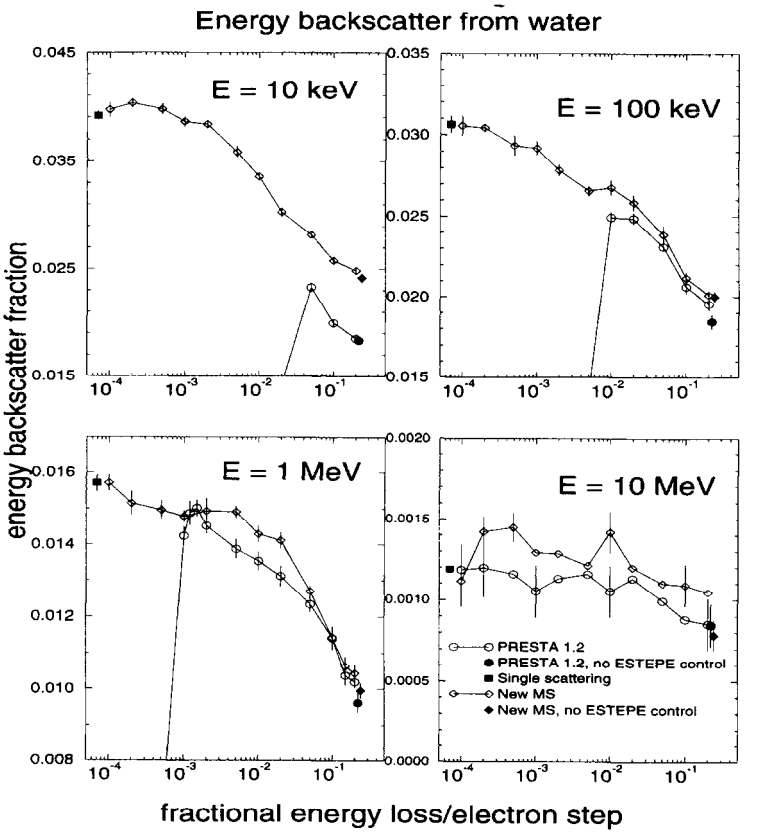

Fig. 14. Energy backscatter from water.

Appendix: Derivation of the Goudsmit–Saunderson series starting from a summation of conditional probabilities

A compound probability distribution comprised of a sum of individual scattering events takes the general form:

$$F(\Theta,\Phi)\sin\Theta\,d\Theta\,d\Phi = e^{-\lambda}\sum_{n=0}^{\infty}\frac{\lambda^n}{n!}f_n(\Theta,\Phi)\sin\Theta\,d\Theta\,d\Phi, \quad (A.1)$$

where λ is the distance measured in the mean-free-paths of a cross section $\sigma(\theta,\phi)$, and $f_n(\Theta,\Phi)$ is the conditional probability of exactly n interactions summing to the cumulative scattering angles Θ and Φ.

The conditional probability $f_n(\Theta,\Phi)$ may be written in terms of the single scattering cross sections as:

$$f_n(\Theta,\Phi) = \left[\prod_{k=1}^{n}\int \sin\theta_k\,d\theta_k\,d\phi_k\,\tilde{\sigma}(\theta_k,\phi_k)\right] \times\delta(\cos\Theta-\cos\theta_{\Sigma_n})\delta(\Phi-\phi_{\Sigma_n}), \quad (A.2)$$

where the normalised cross section is $\tilde{\sigma}(\theta,\phi)=\sigma(\theta,\phi)/\int\sigma(\theta,\phi)\sin\theta\,d\theta\,d\phi$, and θ_{Σ_n} and ϕ_{Σ_n} are distributions of angles that result from exactly n scatterings. The δ-functions select only those angles Θ and Φ that we seek. For the special case $n=0$, the product inside the [ ]-brackets is to be given the value of unity while $\cos\theta_{\Sigma_n}=1$ and $\phi_{\Sigma_n}=0$. Thus:

$$f_0(\Theta,\Phi)=\delta(\cos\Theta-1)\delta(\Phi). \quad (A.3)$$

The double δ-function may be expressed in terms of the spherical harmonics Y_{lm} and thus:

$$f_n(\Theta,\Phi) = \left[\prod_{k=1}^{n}\int \sin\theta_k\,d\theta_k\,d\phi_k\,\tilde{\sigma}(\theta_k,\phi_k)\right] \times\sum_{l=0}^{\infty}\sum_{m=-l}^{l}Y_{lm}^{*}(\Theta,\Phi)Y_{lm}(\Theta_{\Sigma_n},\Phi_{\Sigma_n}). \quad (A.4)$$

Compound angles in spherical harmonics can be expressed in terms of Jacobi polynomials $d^{(l)}$[51]. For n-scatterings:

$$f_n(\Theta,\Phi) = \left[\prod_{k=1}^{n}\int \sin\theta_k\,\mathrm{d}\theta_k\,\mathrm{d}\phi_k\,\tilde{\sigma}(\theta_k,\phi_k)\right] Y^*_{lm_n}(\Theta,\Phi) \times\left\{(-1)^{m_1-m_n}\prod_{j=2}^{n} d^{(l)}_{m_j,m_{j-2}}(\theta_j)\mathrm{e}^{\mathrm{i}m_j\phi_j}\right\} \times Y_{lm_1}(\theta_1,\phi_1), \quad (A.5)$$

where the convention is adopted that repeated indices (in this case $m_1, m_2, \ldots, m_n$) are to be summed from $-l$ to l. For the cases $n = 0, 1$, the product inside the $\{\}$-brackets is to be interpreted as unity, giving the correct terms for no-scattering and single-scattering.

If the cross section distinguished between the two polarisations of the electron, our general considerations would stop here. However, we now consider the case where the cross section does not depend on the polarity of the electron. Thus, $\tilde{\sigma}(\theta,\phi) = \sigma(\theta)/2\pi\int\sigma(\theta)\sin\theta\,\mathrm{d}\theta \equiv \tilde{\sigma}(\theta)/2\pi$ and all the integrations over the ϕ_j may be performed yielding a factor $(2\pi)^n\sum_{j=1}^{n}\delta_{m_j}0$. With the identification $Y_{l0}(\theta,\phi) = \sqrt{2l+1/4\pi}\,P_l(\cos\theta)$ and $d^{(l)}_{(0)}(\theta_j) = P_l(\cos\theta)$ [51],

$$f_n(\Theta,\Phi) = \sum_{l=0}^{\infty}\frac{2l+1}{4\pi}P_l(\cos\theta)\left[\prod_{k=1}^{n}\int\sin\theta_k\,\mathrm{d}\theta_k\,\tilde{\sigma}(\theta_k)\right]^n. \quad (A.6)$$

Substituting Eq. (A.6) into Eq. (A.1) yields exactly the Goudsmit–Saunderson series given in Eq. (2) except for an overall factor of $\frac{1}{2}\pi$ as the Goudsmit–Saunderson series is normalised to unity over integration over the polar angle only, where we have chosen in Eq. (A.1) to normalise to unity with respect to integration over both the polar and azimuthal angles.

References

[1] J.E. Bond, R. Nath and R.J. Schulz, Med. Phys. 5 (1978) 422.
[2] R. Nath and R.J. Schulz, Med. Phys. 8 (1981) 85.
[3] A.C. McEwan and V.G. Smyth, NRL Report Number 1983/7, Christchurch, New Zealand (1983).
[4] A.F. Bielajew, D.W.O. Rogers and A.E. Nahum, Phys. Med. Biol. 30 (1985) 419.
[5] D.W.O. Rogers, A.F. Bielajew and A.E. Nahum, Phys. Med. Biol. 30 (1985) 429.
[6] V.G. Smyth, Med. Phys. 13 (1986) 196.
[7] A.F. Bielajew and D.W.O. Rogers, in: "Monte Carlo Transport of Electrons and Photons", Eds. T.M. Jenkins et al. (Plenum, New York, 1989) 115.
[8] B.J. Foote and V.G. Smyth, Nucl. Instr. and Meth. B 100 (1995) 22.
[9] A.E. Nahum and M. Kristensen, Med. Phys. 9 (1982) 925.
[10] R. Nath, Med. Phys. 9 (1982) 927.
[11] A.C. McEwan and V.G. Smyth, Med. Phys. 11 (1984) 216.
[12] R.J. Schulz and R. Loevinger, Med. Phys. 11 (1984) 217.
[13] V.G. Smyth and A.C. McEwan, Phys. Med. Biol. 31 (1986) 299.
[14] A.F. Bielajew and D.W.O. Rogers, Physics in Medicine and Biology 31 (1986) 301.
[15] A.F. Bielajew and D.W.O. Rogers, Nat. Res. Council of Canada Rep. PIRS-0042 (1986).
[16] A.F. Bielajew and D.W.O. Rogers, Nucl. Instr. and Meth. B 18 (1987) 165.
[17] G.Z. Molière, Z. Naturforsch. 2a (1947) 133.
[18] G.Z. Molière, Z. Naturforsch. 3a (1948) 78.
[19] P. Andreo, J. Medin and A.F. Bielajew, Med. Phys. 20 (1993) 1315.
[20] A.F. Bielajew, Nucl. Inst. and Meth. B 86 (1994) 257.
[21] P. Andreo, Phys. Med. Biol. 36 (1991) 861.
[22] B. Nilsson, A. Montelius and P. Andreo, Med. Phys. 19 (1992) 1413.
[23] D.W.O. Rogers, Med. Phys. 20 (1993) 319.
[24] A. Ferrari, P.R. Sala, R. Guaraldi and F. Padoani, Nucl. Instr. and Meth. B 71 (1992) 412.
[25] J.M. Fernández-Varea, R. Mayol, J. Baró and F. Salvat, Nucl. Instr. and Meth. B 73 (1993) 447.
[26] W. Bothe, Z. Phys. 5 (1921) 63.
[27] G. Wentzel, Ann. Phys. 69 (1922) 335.
[28] S.A. Goudsmit and J.L. Saunderson, Phys. Rev. 57 (1940) 24.
[29] S.A. Goudsmit and J.L. Saunderson, Phys. Rev. 58 (1940) 36.
[30] M.J. Berger and R. Wang, in: "Monte Carlo Transport of Electrons and Photons", eds. T.M. Jenkins et al. (Plenum, New York, 1989) 21.
[31] S.M. Seltzer, in: "Monte Carlo Transport of Electrons and Photons", Eds. W.R. Nelson et al. (Plenum, New York, 1989) 153.
[32] S.M. Seltzer, Int. J. Appl. Rad. Isotopes 42 (1991) 917.
[33] W.R. Nelson, H. Hirayama and D.W.O. Rogers, Stanford Linear Accelerator Center Report SLAC-265 (Stanford, CA, 1985).
[34] A.F. Bielajew, H. Hirayama, W.R. Nelson and D.W.O. Rogers, Nat. Res. Council of Canada Rep. PIRS-0436 (1994).
[35] N.F. Mott, Proc. R. Soc. London A 124 (1929) 425.
[36] N.F. Mott, Proc. R. Soc. London A 135 (1932) 429.
[37] H.A. Bethe, Phys. Rev. 89 (1953) 1256.
[38] K.B. Winterbon, Nucl. Instr. and Meth. B 21 (1987) 1.
[39] M. Abramowitz and I.A. Stegun (Eds.), Handbook of Mathematical Functions with Formulae, Graphs and Mathematical Tables, Appl. Math. Ser. 55 (National Bureau of Standards, Washington, 1964).
[40] G.N. Watson, A Treatise on the Theory of Bessel Functions, 2nd ed. (Cambridge Univ. Press, Cambridge, 1948).
[41] S. Wolfram, Mathematica: A System for Doing Mathematics by Computer (Addison-Wesley, Redwood City, 1991).
[42] W.H. Press et al., Numerical Recipes in ForTran, 2nd ed. (Cambridge Univ. Press, Cambridge, 1992) 963.
[43] A.F. Bielajew, R. Wang and S. Duane, Nucl. Instr. and Meth. B 82 (1993) 503.
[44] M.J. Berger and S.M. Seltzer, NBS Report NBSIR 82-2550-A (second edition) (1983).
[45] ICRU, Report 37, Bethesda MD (1984).
[46] M.J. Berger, NIST Report NISTIR-4999 (Washington, DC) (1992).
[47] D.W.O. Rogers, Nucl. Instr. and Meth. 227 (1984) 535.
[48] C.T. Ballinger, J.A. Rathkopf and W.R. Martin, Nucl. Sci. Eng. 112 (1992) 283.
[49] L.H. Gray, Brit. J. Radiology 10 (1937) 721.
[50] U. Fano, Radiat. Res. 1 (1954) 237.
[51] A.R. Edmonds, Angular Momentum in Quantum Mechanics, 2nd ed. (Princeton Univ. Press, Princeton, NJ, 1960).